

IFUP-TH 34/2000

## Comparison of Transfer-to-Continuum and Eikonal Models of Projectile Fragmentation Reactions

A. Bonaccorso<sup>(a),(b)</sup> and G.F. Bertsch<sup>(a)</sup>

<sup>(a)</sup>Dept. of Physics and Inst. Nuclear Theory

University of Washington, Box 351550

Seattle, WA 98195

<sup>(b)</sup>Istituto Nazionale di Fisica Nucleare, Sez. di Pisa,  
56100 Pisa, Italy

Spectroscopic properties of nuclei are accessible with projectile fragmentation reactions, but approximations made in the reaction theory can limit the accuracy of the determinations. We examine here two models that have rather different approximations for the nucleon wave function, the target interaction, and the treatment of the finite duration of the reaction. The nucleon-target interaction is treated differently in the eikonal and the transfer-to-continuum model, but the differences are more significant for light targets. We propose a new parameterization with that in mind. We also propose a new formula to calculate the amplitude that combines the better treatment of the wave function in the eikonal model with the better treatment of the target interaction in the transfer-to-continuum model.

**PACS** number(s):25.70.Hi, 21.10Gv,25.60Ge,25.70Mn,27.20+n

**Key-words** Breakup, absolute cross sections, eikonal approximation, optical potential, S-matrix, T-matrix.

## 1. Introduction

Heavy ion reactions at intermediate energy offer great promise to measure spectroscopic properties of nuclei far from stability, but one needs a tractable reaction theory to interpret the experiments. In this respect the availability of higher energy heavy ion beams is most welcome, because it becomes a reasonable theoretical approximation to neglect exchange of nucleons between the colliding nuclei. One can therefore consider the interaction in each nucleus as that of an external (complex) potential field. Within the framework of this basic approximation and with given potentials, we will here address the question of the accuracy of further simplified models of the reaction cross sections. A number of theoretical models have been proposed and calculated [1]-[12] in which different approximations were made. In this work we focus on two of the models, the eikonal model [1]-[7] and the transfer-to-the-continuum (TC) model [8]-[12].

There are several cross sections that are measured and calculated in the models. The simplest measurement is the single-neutron removal cross section, in which only the projectile residue, namely the core with one less nucleon, is observed in the final state. Besides the integrated removal cross section, denoted by  $\sigma_{-n}$ , the differential momentum distribution  $d^3\sigma_{-n}/dk^3$  is also measured. A particularly useful cross section is  $d\sigma_{-n}/dk_z$ , the removal cross section differential in longitudinal momentum. If the final state neutron can also be measured, the corresponding coincident cross section  $A_p \rightarrow (A_p - 1) + n$  is called the diffractive breakup cross section. The difference between the removal and diffractive breakup is called the stripping cross section.

This paper is organized as follows. In Sec. II we summarize the essential ingredients of the TC model and the eikonal model, and discuss the accuracy of the neglect of finite interaction times in the eikonal model. In Sect III we discuss the different treatment of the neutron-target S-matrix in the two models. We will not discuss the accuracy of the Hankel function approximation separately, but it of course plays a role in the comparison of cross sections that we make in section IV which contains also our conclusions.

## 2. Theoretical models

All theoretical methods used so far rely on a basic approximation to describe the collision with only the three-body variables of nucleon coordinate, projectile coordinate, and target coordinate. Thus the dynamics is controlled by the three potentials describing nucleon-core, nucleon-target, and core-target interactions. In most cases the projectile-target relative motion is treated semiclassically by using a trajectory of the center of the projectile relative to the center of the target  $\mathbf{s}(t) = \mathbf{b}_c + \mathbf{v}t$  with constant velocity  $v$  in the  $z$  direction and impact parameter  $\mathbf{b}_c$  in the  $xy$  plane. Along this trajectory the amplitude for a transition from a nucleon state  $\psi_i$  to a state  $\psi_f$  is given by

$$A_{fi} = \frac{1}{i\hbar} \int_{-\infty}^{\infty} dt \langle \psi_f(t) | V_{nt}(\mathbf{r}) | \psi_i(t) \rangle, \quad (1)$$

where  $V_{nt}$  is the neutron-target interaction. The state  $\psi_i$  will be the bound state of the nucleon in the projectile, while the final state  $\psi_f$  is a continuum state. The detailed derivation of Eq.(1) from a scattering amplitude containing the full time dependent propagator can be found in Sec.II of Ref. [9]. There it was shown to hold under the hypothesis

that the breakup process is limited to peripheral projectile-target trajectories and that it is due mainly to the neutron interaction with the target potential. The probabilities for different processes can be represented in terms of the amplitude as

$$\frac{dP}{d\xi} = \sum |A_{fi}|^2 \delta(\xi - \xi_f), \quad (2)$$

where  $\xi$  can be momentum, energy or any other variable for which one measures a differential cross section.

The effects associated with the core-target interaction will be included by multiplying the above probability by the  $b_c$ -dependent probability for the core to be left in its ground state.

Thus the differential cross sections with respect to the longitudinal momentum is

$$\frac{d\sigma}{dk_z} = C^2 S \int_0^\infty d\mathbf{b}_c \frac{dP_{-n}(k_z, b_c)}{dk_z} P_{ct}(b_c), \quad (3)$$

where  $k_z$  is the (longitudinal) recoil momentum of the neutron (see Eq. (2.3) of [11]) and  $C^2 S$  is the spectroscopic factor for the initial single particle orbital. The cross section can be further divided into a stripping cross section  $\sigma_{str}$  and a diffractive breakup cross section  $\sigma_{diff}$  depending on whether the removed neutron is detected in the final state or not. We accordingly will consider these individual probability distributions,

$$P_{-n} = P_{str} + P_{diff}, \quad (4)$$

and use a similar notation for the cross sections.

We first summarize the transfer-to-the-continuum (TC) model. This model treats the time-dependence of the reaction explicitly, thus conserving energy. It uses the on-shell neutron-target scattering matrix, therefore making it in principle model-independent with respect to that interaction. It also makes use of the asymptotic form of the neutron wave function in the projectile. This is an asset in that the formulas have an analytic limit, but a disadvantage in that the results are only reliable at peripheral impact parameters<sup>1</sup>. The two breakup probabilities are given by the following expressions:

$$\frac{dP_{diff}(b_c)}{dk_z} = \sum_{l_n} |1 - S_{l_n}|^2 B(l_n, k_z, b_c), \quad (5)$$

$$\frac{dP_{str}(b_c)}{dk_z} = \sum_{l_n} (1 - |S_{l_n}|^2) B(l_n, k_z, b_c), \quad (6)$$

where the factor  $B(l_n, k_z, b_c)$  is a transfer probability which depends on the details of the initial and final states, and on the energy of relative motion. It is given by

$$B(l_n, k_z, b_c) = \frac{1}{2} \left( \frac{\hbar}{mv} \right) \frac{1}{k_f} (2l_n + 1) |C_i|^2 \frac{e^{-2\eta b_c}}{2\eta b_c} M_{l_n l_i}, \quad (7)$$

<sup>1</sup> The derivation of the TC model requires that the neutron-target and the neutron-projectile potentials do not overlap. In this respect the result that can be expressed entirely in terms of asymptotic properties reminds one of Bég's theorem[13].

where  $l_i$  is the angular momentum of the bound neutron in the initial state with respect to the core. The variable  $l_n$  has the interpretation as the angular momentum of the neutron with respect to the target. Also

$$M_{l_n l_i} = \frac{1}{\sqrt{\pi}} \int_0^\infty dx e^{-x^2} P_{l_i}(X_i + B_i x^2) P_{l_n}(X_f + B_f x^2), \quad (8)$$

The arguments of the Legendre polynomials  $P_{l_i}$  and  $P_{l_n}$  are  $X_i = 1 + 2(k_z/\gamma_i)^2$  and  $X_f = 2((k_z - mv)^2/(\gamma_i^2 + 2mvk_z - (mv)^2) - 1)$ ,  $B_i = 2\eta/d\gamma_i$  and  $B_f = 2\eta/dk_f$ .  $\gamma_i$  is related to the initial state binding energy by  $\gamma_i = \sqrt{-2m\varepsilon_i/\hbar}$ . The variable  $\eta = \sqrt{k_z^2 + \gamma_i^2}$  has the interpretation as the modulus of the transverse component of the neutron momentum. In our notation  $\varepsilon_f$  is the energy of the neutron relative to the target in the final state. For diffraction this is the same as the final laboratory energy of the neutron if the target recoil kinetic energy is neglected. In the case of stripping, if it goes through compound nucleus formation,  $\varepsilon_f$  is the excitation energy of the compound state above the neutron threshold in the residual nucleus. For inelastic scattering it is the energy of the breakup neutron before it scatters from the target. This is equivalent to the sum of the excitation energy of the target final state and the final neutron energy relative to the target. If the target recoil kinetic energy is neglected the final kinetic energy  $E_f$  of the ejectile is given by the energy conservation condition

$$E_f - E_{inc} = Q = \varepsilon_i - \varepsilon_f, \quad (9)$$

where  $E_{inc}$  is the initial incident energy of the projectile in the laboratory,  $Q$  is the reaction  $Q$  value given by  $Q = \varepsilon_i - \varepsilon_f$  and  $\varepsilon_i$  is the initial neutron binding energy in the projectile. With this approximation Eq. (9) relates  $k_z$  to the the projectile residue parallel momentum. Finally,  $|C_i|^2$  is the asymptotic normalization constant of the initial bound wave function

$$\psi_i(r) = -i^l C_i \gamma_i h_{l_i}^{(1)}(i\gamma_i r) Y_{l_i m_i}(\theta, \phi), \quad \gamma_i r \gg 1. \quad (10)$$

It is obtained by fitting a realistic radial wave function to the Hankel form  $h_{l_i}^{(1)}$  outside the potential radius. In this way the transfer to the continuum results are model dependent. On the other hand the dimensionless quantity  $\Lambda_{l_i} = \gamma_i^{-1} |C_i|^2 C^2 S$  has been called reduced normalization in the contest of spectroscopy done with transfer reactions [14,15]. If one considers  $\Lambda_{l_i}$  as the prefactor of the theoretical cross section obtained with the Hankel function, the ratio between the experimental cross section and the theoretical cross section would determine its value.

Eqs.(5-7) were derived assuming no overlap between neutron-core and neutron-target potential. This assumption can be avoided if one makes an eikonal approximation to the basic expression for the amplitude, Eq.(1), as shown in Appendix B. Then one derives [4,10]

$$\frac{dP_{-n}(b_c)}{dk_z} \sim \frac{1}{2\pi} \int_0^\infty d\mathbf{b}_n \left[ |(1 - e^{-i\chi(b_n)})|^2 + 1 - |e^{-i\chi(b_n)}|^2 \right] |\tilde{\psi}_i(\mathbf{b}_n - \mathbf{b}_c, k_z)|^2, \quad (11)$$

where  $\mathbf{b}_n$  is the transverse coordinate of the neutron with respect to the target. The neutron-target  $S$ -matrix is approximated by the eikonal form  $\bar{S}(b_n) = e^{-i\chi(b_n)}$ , related to the optical potential  $V_{nt}$  by

$\chi(\mathbf{b}_n) = \frac{1}{\hbar v} \int_{-\infty}^{\infty} V_{nt}(x, y, z') dz'$ . Finally,  $|\tilde{\psi}_i(\mathbf{b}_n - \mathbf{b}_c, k_z)|^2$  is the longitudinal Fourier transform of the initial state wave function. Also the connection between Eqs.(5-7) and Eq.(11) is made by replacing the sum over partial waves in Eqs.(5,6) by the integral over impact parameters as in Eq.(11), and by evaluating the longitudinal Fourier transform in Eq.(11) using the asymptotic initial state wave function, Eq.(10). The one-dimensional Fourier transform of the initial wave function can be calculated analytically in the case of an Hankel function approximation Eq.(10) yielding

$$\begin{aligned} \frac{1}{(2l_i + 1)} \sum_{m_i} |\tilde{\psi}_{l_i m_i}(\mathbf{b}_c - \mathbf{b}_n, k_z)|^2 &= \frac{1}{(2l_i + 1)} \sum_{m_i} |2C_i Y_{l_i, m_i}(\hat{k}_z) K_{m_i}(\eta\rho)|^2 \\ &\approx C_i^2 \frac{e^{-2\eta\rho}}{2\eta\rho} P_{l_i}(X_i), \end{aligned} \quad (12)$$

where  $\rho = |\mathbf{b}_c - \mathbf{b}_n|$ .

The total breakup probability is obtained from the integral of Eq.(11) involving

$$I(k_z^{min}, k_z^{max}) = \int_{k_z^{min}}^{k_z^{max}} dk_z |\bar{\psi}_i(\mathbf{b}_n - \mathbf{b}_c, k_z)|^2. \quad (13)$$

$k_z^{min}$  and  $k_z^{max}$  are the kinematically allowed minimum and maximum neutron parallel momenta discussed in the following. Therefore although Eq.(11) describes the neutron-target rescattering in the eikonal approximation, it still satisfies neutron energy and momentum conservation.

On the other hand, a sudden approximation or frozen halo form of the eikonal method has been used in [1,6,5] where energy conservation was neglected. This approximation can be derived from Eq.(11) when the integration limits in Eq.(13) can be extended to  $\pm\infty$ . Then Eq.(13) is just be the longitudinal density, and the formulae for the TC and eikonal model become identical. In fact in this limit the removal cross section reduces to

$$\sigma_{-n} = C^2 S \int d^2 \mathbf{b}_c \int d^3 \mathbf{r}_n \left[ |(1 - \bar{S})|^2 + 1 - |\bar{S}|^2 \right] |S_{ct}(b_c)|^2 |\psi_i(\mathbf{b}_n - \mathbf{b}_c, z)|^2, \quad (14)$$

which is consistent with the breakup cross section of [1,6]. In Eq.(14)  $\bar{S}$  is an eikonal S-matrix, as defined after Eq.(11).

The steps necessary to obtain Eq.(14) from Eq.(11) and Eqs.(4-6) can be justified in the high energy limit as follows. If the neutron binding energy is not too large, the final energy or momentum distributions are strongly peaked at the incident energy per nucleon. Therefore it is possible to average the dependence of the neutron target optical model S-matrix of Eqs.(5,6) over the full range of neutron continuum energies and assume that the S-matrix can be approximated with the eikonal values  $\bar{S}$  obtained at  $\varepsilon_f = \frac{1}{2}mv^2$ . On the other hand, for the eikonal approximation to be good it is necessary that the parallel component of the neutron momentum  $k_z$  be large with respect to the transverse component  $\eta$ . In particular such condition must be satisfied for the minimum values of both. From the definition of  $k_z$  it is easy to see that its lowest possible value is  $k_z^{min} = -(\varepsilon_i + \frac{1}{2}mv^2)/(\hbar v)$  in correspondence to  $\varepsilon_f = 0$ . And that the minimum value of  $\eta = \gamma_i$ . Therefore we get  $|k_z^{min}| \gg \gamma_i$  if  $\sqrt{E_{inc}}/2 \gg \sqrt{\varepsilon_i}$ . For a real halo with separation energy around 0.5MeV the condition  $|k_z^{min}| \gg \gamma_i$  is satisfied at all initial

energies. Increasing the binding energy it is necessary to go to higher incident energies in order for the parallel momentum component to be larger than the transverse one. For a typical binding of 10MeV or more the conditions for the sudden eikonal approximation to be valid are satisfied from about 80A MeV. It is useful also to consider the values of neutron-target center of mass momentum  $k_v = \mu v/\hbar$  where  $\mu = A_t/(A_t + 1)$  is the neutron-target reduced mass. Here too we see that for a typical diffuseness of  $a=0.5\text{fm}$  the semiclassical condition  $ak_v \gg 1$  is satisfied starting from about 80MeV. Finally if such condition is satisfied we can extend the lower limit in the  $k_z$  integral to  $-\infty$ . There is however also an upper limit to the final neutron or ejectile momentum value in the parallel direction, due to the energy and momentum conservation. It was discussed in ref.[16] where it was shown that

$$k_z^{max} = \left(1 - \frac{1}{2A_p}\right) m, \quad (15)$$

$m$  is the neutron mass.  $k_z^{max} = 0.96 fm^{-1}$  for a  $^{12}\text{Be}$  projectile. In terms of the maximum neutron final energy in the continuum the above condition reads

$$\varepsilon_f^{max} = k_z^{max} \hbar v + \frac{1}{2} m v^2 + \varepsilon_i. \quad (16)$$

If this upper limit is also extended to  $+\infty$  then the  $k_z$  integral gives a  $\delta$ -function and inserting Eq.(11) and the damping factor  $P_{ct} = |S_{ct}|^2$  in Eq.(3) we finally get Eq.(14).

These very strict conditions necessary to extend the theoretical limits of the  $k_z$  integral to infinity, can be somewhat revised in practical calculations. To see how accurate the sudden approximation is, we have calculated the integral  $I(k_z^{min}, k_z^{max})$  under various conditions of angular momentum, neutron binding energy in the projectile, and projectile velocity. For values of the parameters of interest there can be a rather large reduction for small values of the neutron transverse radius in the projectile,  $|b_n - b_c|$ . However, the approximation becomes increasingly accurate as the transverse radius is made larger. In Fig. 1 we show the regions of energies in which the ratio

$$R = \frac{I(-\infty, \infty)}{I(k_z^{min}, k_z^{max})},$$

is within 5%, 5-10% and 10% of being unity, for a  $d$ -wave orbital at a transverse radius corresponding to strong absorption. The region of good agreement is somewhat larger for  $s$ - and  $p$ -waves. Thus it seems that the sudden approximation should be acceptable for weakly bound neutron orbitals ( $< 6\text{MeV}$ ) and beam energies greater than 40A MeV, provided the reaction samples the initial wave function at distances rather larger than the sum of the radii of the reaction partners.

It must be noted that here as in Eq.(3) we have adopted the so called no-recoil approximation [3] which consists in factorizing out from the matrix element the core-target S-matrix. Another important remark has to do with the extension of the lower limit in the  $k_z$  integral to  $-\infty$ . Values of  $k_z$  smaller than  $k_z^{min}$  obtained when  $\varepsilon_f = 0$  would correspond to final states in the projectile below the breakup threshold for the diffraction term. For the stripping term they would correspond to final bound states in the target.

Taking  $k_z^{min} \rightarrow -\infty$  is analogous to the completeness relation introduced in [1]. For this reason in Eq.(14) the diffraction term has usually been corrected by subtracting terms like  $|\langle \psi_i | 1 - \bar{S} S_{ct} | \psi_i \rangle|^2$ . In the transfer to the continuum model this correction is not as important because the neutron final energy is always positive and the  $k_z$  integration is performed in the kinematically allowed region.

Estimates of absolute breakup cross sections published so far have been made either using Eq.(3) with the breakup probability given by the transfer to the continuum theory Eqs.(4-8) [10–12] or with Eq.(14) [1,2,5,7,17]. There are a number of assumptions contained in both models, the validity of which we are going to study in this paper.

### 3. n-target optical potential and S-matrix

Experimentalists often use light targets such as  ${}^9\text{Be}$  or  ${}^{12}\text{C}$  to study spectroscopy by projectile fragmentation reactions. The definition of an optical potential for light targets is a very delicate issue which has been discussed in the literature for long time [18]. There are two main issues, i) global parameterizations are based on large nuclei; ii) the imaginary optical potential changes drastically for light nuclei. Recently these problems have been faced in the contest of halo breakup studies [5,11,12] where different choices have been made by different authors. Bertsch et al.[2] used the Varner et al. parameterization [19]. Such parameterization has been obtained taking into account relatively low energy proton and neutron cross sections (10-26MeV) on heavy targets,  $A=40-209$ . In ref.[5] a neutron target S-matrix was constructed in the optical limit of Glauber theory. The corresponding optical potential does not need to be given explicitly, but the behavior of the transmission coefficient given in [5] would suggest a strongly absorbing potential of volume type. Bonaccorso [11] extended to high energies a parameterization of a phenomenological n- ${}^9\text{Be}$  optical potential fitted to low energy data. This potential seemed however to overestimate the free particle cross sections at high energies [11] and therefore ref.[12] also considered a microscopic optical potential calculated according to the method of Jeukenne, Lejeune and Mahaux (JLM) [18]. The JLM potentials are more complicated to calculate and to use than a simple standard parameterization. Then for the purpose of the present paper we have attempted to fit the available experimental n- ${}^9\text{Be}$  total cross sections with a new potential of the standard form. The potential is given by a real Woods-Saxon well and it has both volume and a surface derivative Woods-Saxon forms for the imaginary part. In obtaining the parameters given in Table I we have been guided by some existing parameterizations [20,21] obtained by fitting low energy data. We have modified such parameterizations to get a smooth behavior of the free particle neutron- ${}^9\text{Be}$  cross section in the energy range 10-180 MeV. The free-particle cross section have been obtained in an optical model calculation. A good agreement of calculated free neutron angular distributions with the data of ref.[20] has also been obtained. This potential satisfies very well the subtracted dispersion relations as given for example in Ref.[22] at energies larger than 40MeV. For lower energies the agreement is less good at small radii.

In Fig. 2, top left, we show the experimental cross sections [23] together with the optical model cross sections, where the full curve is the total cross section, the dot-dashed curve is the elastic cross section while the dashed curve is the reaction cross section. At the bottom left we show the same quantities calculated in the eikonal approximation. The effect of the

eikonal approximation is to reduce the calculated cross sections, in particular at the lower energies. The reduction is more pronounced for the elastic cross section, probably because quantum mechanical reflection effects on the potential barrier can not be reproduced by the eikonal approximation. For comparison we show at the top right and bottom right respectively the same quantities calculated with the Varner parameterization. Varner potential does not reproduce the high energy data, also it gives a dominance of the elastic scattering up to about 80MeV. Here too the eikonal calculations underestimate the elastic scattering at low energies.

Our potential has a rather strong surface term. It gives also large volume integrals ( $J_W/A \approx 200 \text{ MeV fm}^3$ ) in accordance with the light nuclei systematics[18,24]. The microscopic origin of it can be understood since  ${}^9\text{Be}$  is weakly bound and it has rather high breakup probability. Also it has been known for long time [25] to have an unusually large mean square radius and to be strongly deformed. Finally we notice that we get a very large elastic vs reaction cross section ratio at low energy. The JLM potential gives the same behavior. The little experimental free particle data available show similar trend and it would be interesting to see if breakup reactions around 20A MeV which will soon be feasible at GANIL, will parallel such a behavior.

In Fig. 3 we show the behavior of the term  $|1 - S|^2$  and of the transmission coefficient  $1 - |S|^2$  when calculated by the optical model (solid and dashed line respectively) and by the eikonal approximation (dotted and dot-dashed line). The results are shown as a function of the angular momentum  $l_n$  and in the case of the eikonal calculations the semiclassical relation  $l_n + 1/2 = kb_n$  was used to make the connection between the angular momentum and the neutron impact parameter. We give results at energies ranging from 20 to 100 MeV. An interesting characteristic of these results is that the eikonal seems to concentrate the scattering at larger impact parameters than in the optical model case. Such effects have been seen by other authors [26] in different situations than ours and sometimes it has also been shown [7,26] that higher order eikonal corrections can improve the agreement with the quantum mechanical calculations. It is possible that in our case the effect is amplified by the deep surface part of the imaginary potential. It is well known that the eikonal approximation works well in the presence of strongly absorbing volume potentials and differences would also be less extreme for potentials that have more diffuse edges. This is because the reflection effects at the barrier that modify the neutron trajectory are not taken into account in a semiclassical approach.

From the differences seen here, we would expect quite large differences between predictions of the two treatments of the S-matrix. The quantification of these differences is the subject of section IV.

#### 4. Cross sections and conclusions

We start this section by showing some results for the total probability  $P(b_c) = P_{-n}(b_c)P_{ct}(b_c)$  obtained from the integrand of Eq.(3) after integrating over  $k_z$  and using Eq.(18). The  $R_s$  values are given in Table III at each energy. They were obtained, as explained in Appendix A, from the S-matrix calculated by folding the neutron-target optical potential of Table I with the projectile density, at all energies but 20A MeV. At such a low energy the optical limit of the eikonal model cannot be justified, but calculations

by Carstoiu [27] in second order eikonal approximation, folding the JLM potentials agree with our  $R_s$  at all energies, including 20A MeV. Same values are also obtained from the optical potential of [28].

For our numerical comparison of the various methods, we have chosen to study the breakup from the s and p states in  $^{12}\text{Be}$  which were recently measured by Navin et al.[17]. The initial bound state parameters are given in Table II.

In Fig. 4 we show the total probabilities for diffraction obtained in the TC calculation by the solid lines. The dashed lines are for the absorption or stripping. Energies are as in Fig. 3. The dotted lines are the calculations from the diffraction integrand of Eq.(11) while the dot-dashed lines are for the stripping. Because of the shift in the S-matrices of Fig. 3, we see here that the eikonal calculations have their maxima at slightly larger core-target distances than the optical model calculations. At the lowest energy the optical model gives almost equal diffraction and stripping probabilities. The eikonal calculation gives a rather larger diffraction probability. In all other cases the stripping is the dominant term. This effect was first pointed out in normally bound nuclei [29,30] and it has been confirmed by some experiments [31] and other theoretical calculations [12].

The TC calculations discussed in this paper are performed using the asymptotic, Hankel form of the initial state wave function, which can be the origin of some divergence if the projectile and target potential have an important overlap during the reaction. This problem was discussed in great detail in Ref.[9] where it was shown to be more important for the stripping term since it is proportional to the neutron target phase shift, while the diffraction term, being proportional to the square of the phase shift converges more rapidly. This situation reflects the fact that diffraction reactions involve a more peripheral part of the initial wave function than stripping reactions. Here we can easily see from Eq.(11) that the integral over  $b_n$ , the neutron target impact parameter is well behaved provided the neutron-target potential and the corresponding S-matrix fall off more rapidly than the tail of the initial wave function. A practical way to satisfy such a condition and to avoid any divergence in the sum over neutron partial waves in Eq.(6) is to use a small value for the diffuseness of the imaginary part of the optical model (cf. Sec.IV of [9]). Otherwise, as it is shown in Appendix B it is possible to start again from Eq.(1) and obtain a formula which contains the realistic single particle wave function and an optical model S-matrix, still keeping the information on the proper kinematical limits for the neutron parallel momentum. The only hypothesis involved is that high neutron angular momenta are dominant.

To show the amount of error that is introduced by the Hankel approximation in the TC method, we show in Fig. (5) the integrand functions of the stripping and diffraction terms of Eq.(11), after integrating over  $k_z$ , obtained from the realistic bound state wave function and the corresponding terms in the sum over partial waves of Eqs.(5,6) in the case of the incident energy of 78A MeV. The calculations were done at the fixed impact parameter  $b_c = 5.6\text{fm}$  between the projectile and target. Left figure is for the diffraction term while right figure is for the stripping term. We can see that the calculation for stripping according to Eq. (6) which is done with the Hankel function and optical model S-matrix (diamonds) shows a slower decrease in the interior of the projectile ( small  $b_n$  ) than the calculation with the realistic wave function (crosses) done according to Eq.(27) of Appendix B. Therefore the comparison between these two results gives an

indication of the effect of the Hankel function approximation. On the other hand the eikonal calculations (full curve), done with the full wave function have higher maxima which occur at a larger distance than the optical model calculation. This effect is due to the behavior at large impact parameters of the eikonal S-matrix, as we have discussed before. The comparison of the full curve with the crosses gives an indication of the effect of the eikonal approximation. In the end the integrated probabilities obtained with the three possible approximations contained in Eqs. (5) and (6), Eq.(27) and Eq.(24) differ by not more than about 10%. This leads to about 20% difference in the total cross sections because of the further integration over  $b_c$ , the core-target impact parameter. From the peak values of the diffraction and stripping curves it is easy to see that the stripping is almost three times larger than the diffraction.

The values of the total cross sections are given in Table III. Because the eikonal probabilities are shifted towards larger distances we get total cross sections which are larger by about 20% than the TC calculations at all energies but 20A MeV. At this lowest energy two effects tend to compensate each other: the eikonal free particle cross section is largely underestimated while there is an overestimate of the phase space kinematically allowed. Then the eikonal and optical model calculations seem to give very close results.

Considering all the effects discussed above we conclude than present models used to calculate the breakup cross section might tend to overestimate the true value, but the error should be of the order of 20% or less. On the other hand presently available experimental data are inclusive with respect to the target which was unobserved. In the case of  ${}^9\text{Be}$  it is possible that some part of the cross section comes from reactions in which the target itself underwent breakup. These reactions could account for about 20% of the measured cross sections and they are certainly not taken into account by presently available theoretical models. We suggest therefore that future experiments detect the final excitation state of the target in coincidence with breakup events (as done for example in Ref.[31] for "normal" heavy ions) and at the same time that theoretical models be improved through a more realistic treatment of the core-target interaction, as mentioned in Sec.IV and in Appendix A. We propose also an improved calculation of the breakup amplitude using the new formula Eq.(27) derived in Appendix B that combines the better treatment of the wave function in the eikonal model with the better treatment of the target interaction in the transfer-to-continuum model. We leave to a future study to apply this equation to the reaction data.

Ejectile momentum distributions are not shown in this paper. They have been discussed in great detail in [10–12] where it was shown that there can be noticeable differences in the results of the TC and eikonal methods. Present data do not have enough statistics to distinguish clearly between the two models.

### Acknowledgments

This research was supported by the U.S. Department of Energy under Grant DE-FG03-00-ER41132. We wish to thank David Brink for several discussions and suggestions, Florin Carstoiu for communicating his results before publication and Juan Carlos Pacheco for checking that our n-target optical potential satisfies the dispersion relations.

## A. Ion-ion S-matrix

We discuss here the theory of the core-target S-matrix, needed to calculate  $P_{ct}(b_c)$  in Eq.(3). The best source of information comes from the ion-ion reaction cross section which is related to the core-target S-matrix by

$$\sigma_R^{ct} = \int_0^\infty d^2\mathbf{b}_c (1 - |S_{ct}(\mathbf{b}_c)|^2). \quad (17)$$

Here we have assumed that the semiclassical replacement of the partial wave sum by an integral over  $\mathbf{b}_c$  is permitted. Unlike the nucleon-nucleus scattering, this is always a good approximation, because of the smaller wave length involved, and one can safely calculate this S-matrix in the eikonal approximation. The usual procedure is to define an optical potential for the core-target scattering, and calculate the S-matrix from it. In practice the behavior of the S-matrix is determined by two parameters. The first and most important is the strong absorption radius  $R_s$ , defined as the distance of closest approach for a trajectory that is 50% absorbed from the elastic channel. The reaction cross section practically speaking is determined by the strong absorption radius. The next most important parameter is the thickness  $a$  of the absorption region. In optical model fits, it is closely related to the asymptotic behavior of the imaginary potential  $W(r) \sim e^{(-r/a)}$ . Just as the reaction cross section strongly constrains the strong absorption radius, measurements of the elastic angular distribution provide information about  $a$ .

In this work we shall use a simple parameterized form [11] for  $P_{ct}(\mathbf{b}_c)$ , namely

$$P_{ct}(b_c) = \exp(-\ln 2 e^{(R_s - b_c)/a}). \quad (18)$$

It would be correct to use the elastic scattering S-matrix if the experimental cross sections were reported for projectile breakup leaving the target in its ground state. In fact the target final state is difficult to measure and most experimental cross sections are inclusive with respect to the target final state. Thus the measured cross sections should be somewhat larger than one would calculate with an elastic core-target S-matrix.

A way to include absorption of the projectile core without regard to the target is to construct an optical potential convolution of a nucleon-ion potential with the target density. In the calculations of this work we have determined strong absorption radii by this method, using the optical potential of Sec. III. We also take a diffuseness parameter  $a = 0.6fm$ .

## B. Breakup Amplitude

In this section we give a more general formulation of the breakup problem which is less dependent on the reaction model assumptions of the text. We start with Eq. (1), again assuming a straight-line trajectory. Using a Galilean transformation for the initial wave function as described in ref.[9], Eq. (1) becomes

$$A_{fi} = \frac{1}{i\hbar v} \int d\mathbf{b}_n dz \phi_f(\mathbf{r}) V_{nt}(\mathbf{r}) e^{ik_{fz}z} \tilde{\phi}_i(\mathbf{b}_n - \mathbf{b}_c, k_z), \quad (19)$$

where  $k_z = k_1 = -(\varepsilon_i - \varepsilon_n + \frac{1}{2}mv^2)/(\hbar v)$  and  $k_{fz} = k_2 = -(\varepsilon_i - \varepsilon_n - \frac{1}{2}mv^2)/(\hbar v)$  are the  $z$ -components of the neutron momentum in the initial and final state respectively.

Introduce now a T-matrix in a mixed representation as

$$T(\mathbf{k}_n, \mathbf{b}_n, k_2) = \frac{1}{i\hbar v} \int dz \phi_f(\mathbf{b}, z) V_{nt}(\mathbf{b}, z) e^{ik_2 z}, \quad (20)$$

where  $\mathbf{k}_n$  is the neutron final (measured) momentum.

If the eikonal approximation for the final wave function is used

$$\phi_f^*(\mathbf{b}, z) = e^{-i\mathbf{q}_\perp \cdot \mathbf{b}_n} e^{-iq_z z} e^{\frac{i}{\hbar v} \int_{+\infty}^z V_{nt}(x, y, z') dz'}, \quad (21)$$

the  $dz$  integral in Eq.(20) can be calculated by parts when the initial binding energy is small and the final neutron energy is close to the neutron incident energy and the neutron scattering angle is small such that  $k_2 - q_z \simeq 0$ . Then

$$\frac{i}{\hbar v} \int dz e^{i(k_2 - q_z)z} V_{nt}(\mathbf{b}_n, z) e^{\frac{i}{\hbar v} \int_{-\infty}^z e^{i(k_2 - q_z)z'} V_{nt}(x, y, z') dz'} = 1 - e^{-i\chi(\mathbf{b}_n)}, \quad (22)$$

where

$$\chi(\mathbf{b}_n) = \frac{1}{\hbar v} \int_{-\infty}^{\infty} e^{i(k_2 - q_z)z'} V_{nt}(x, y, z') dz' \approx \frac{1}{\hbar v} \tilde{V}_{nt}(\mathbf{b}_n, 0), \quad (23)$$

where  $V_{nt}$  is a complex potential whose real and imaginary strengths are negative. We finally obtain the breakup amplitude in the eikonal form as

$$A_{fi} = \int_0^\infty d\mathbf{b}_n e^{-i\mathbf{q}_\perp \cdot \mathbf{b}_n} \left(1 - e^{-i\chi(\mathbf{b}_n)}\right) \tilde{\phi}_i(\mathbf{b}_n - \mathbf{b}_c, k_z). \quad (24)$$

Similarly a more general T-matrix in a mixed representation can be obtained starting from the partial wave form

$$T(\mathbf{k}_n, \mathbf{k}_\perp, k_2) = \frac{\hbar^2}{2m} \frac{4\pi}{2ik_n} \sum_{l_n} (2l_n + 1) (S_{l_n} - 1) P_{l_n}(\hat{\mathbf{k}}_n \cdot \hat{\mathbf{k}}_\alpha), \quad (25)$$

on the energy shell such that  $k_n = k_\alpha$ , and defining

$$\begin{aligned} T(\mathbf{k}_n, \mathbf{b}_n, k_2) &= \int \frac{d\mathbf{k}_\perp}{(2\pi)^2} e^{-i\mathbf{k}_\perp \cdot \mathbf{b}_n} T(\mathbf{k}_n, \mathbf{k}_\perp, k_2) \\ &= \frac{\hbar^2}{2m} \frac{4\pi}{2ik_n} \sum_{l_n} (2l_n + 1) (S_{l_n} - 1) \\ &\quad \times \int \frac{d\mathbf{k}_\perp}{(2\pi)^2} e^{-i\mathbf{k}_\perp \cdot \mathbf{b}_n} P_{l_n}(\hat{\mathbf{k}}_n \cdot \hat{\mathbf{k}}_\alpha). \end{aligned} \quad (26)$$

This is unfortunately off shell but we will do the following high energy approximations similar to what we have done above in the eikonal case. In the large angular momentum, small scattering angle limit, define  $b'_n = \frac{(l_n + \frac{1}{2})}{k_n}$ , we can substitute the partial wave sum with an integral and also use  $P_{l_n}(\hat{\mathbf{k}}_n \cdot \hat{\mathbf{k}}_\alpha) \rightarrow J_0(|\mathbf{k}_n - \mathbf{k}_\alpha|b') = (2\pi)^{-1} \int d\phi e^{-i(\mathbf{q}_\perp - \mathbf{k}_\perp) \cdot \mathbf{b}'_n}$  where  $\mathbf{q}_\perp$  is the transverse component of  $\mathbf{k}_n$ . Then

$$\begin{aligned}
A_{fi} &= \frac{1}{i\hbar v} \int d\mathbf{b}_n \int \frac{d\mathbf{k}_\perp}{(2\pi)^2} e^{-i\mathbf{k}_\perp \cdot \mathbf{b}} T(\mathbf{k}_n, \mathbf{k}_\alpha) \tilde{\phi}_i(\mathbf{b}_n - \mathbf{b}_c, k_1) \\
&= \frac{1}{i\hbar v} \frac{\hbar^2}{2m} \frac{4\pi}{2ik_n} \Sigma_{l_n} (2l_n + 1) (S_{l_n} - 1) \\
&\quad \times \int d\mathbf{b}_n \int \frac{d\mathbf{k}_\perp}{(2\pi)^3} \int d\phi e^{-i(\mathbf{q}_\perp - \mathbf{k}_\perp) \cdot \mathbf{b}'_n} e^{-i\mathbf{k}_\perp \cdot \mathbf{b}} \tilde{\phi}_i(\mathbf{b}_n - \mathbf{b}_c, k_z) \\
&\approx -\frac{\hbar k_n}{mv} \int d\mathbf{b}'_n e^{-i\mathbf{q}_\perp \cdot \mathbf{b}'_n} (S_{l_n} - 1) \int d\mathbf{b}_n \int \frac{d\mathbf{k}_\perp}{(2\pi)^2} e^{-i\mathbf{k}_\perp \cdot (\mathbf{b}_n - \mathbf{b}'_n)} \tilde{\phi}_i(\mathbf{b}_n - \mathbf{b}_c, k_z) \\
&= \int d\mathbf{b}_n e^{-i\mathbf{q}_\perp \cdot \mathbf{b}_n} (1 - S_{l_n}) \tilde{\phi}_i(\mathbf{b}_n - \mathbf{b}_d, k_z). \tag{27}
\end{aligned}$$

This formula combined the improved treatment of the interaction by the TC theory with the better treatment of the neutron wave function by the eikonal theory.

## REFERENCES

1. K. Yabana, Y. Ogawa and Y. Suzuki, Nucl. Phys. **A539**, 295 (1992).
2. K. Hencken, G. F. Bertsch and H. Esbensen, Phys. Rev. C **54**, 3043 (1996).
3. G.F. Bertsch, K. Hencken and H. Esbensen, Phys. Rev. C **57**, 1366 (1998).
4. A. Bonaccorso and D. M. Brink, Phys. Rev. C **57**, R22 (1998).
5. J. A. Tostevin, J. Phys. G **25**, 735 (1999).
6. H. Esbensen and G. F. Bertsch, Phys. Rev. C **59**, 3240 (1999).
7. F. Negoita et al., Phys. Rev. C **59**, 2082 (1999).
8. A. Bonaccorso and D. M. Brink, Phys. Rev. C **38**, 1776 (1988).
9. A. Bonaccorso and D. M. Brink, Phys. Rev. C **43**, 299 (1991).
10. A. Bonaccorso and D. M. Brink, Phys. Rev. C **58**, 2864 (1998).
11. A. Bonaccorso, Phys. Rev. C **60**, 054604, (1999).
12. A. Bonaccorso and F. Carstoiu, Phys. Rev. C **61** 034605, (2000).
13. M. A. B. Bég, Ann. Phys. **13**, 110 (1961).
14. G. R. Satchler, *Direct Nuclear Reactions*, Clarendon Press, Oxford 1983. Pag 715.
15. J. Rapaport and A. K. Kerman, Nucl. Phys. **A119** , 641 (1968).
16. T. Fujita and J. Hüfner, Nucl. Phys. **A343**, 493 (1980).
17. A. Navin et al., Phys. Rev. Lett. **85**, 266 (2000).
18. J. P. Jeukenne, A. Lejeune and C. Mahaux, Phys. Rev. C **16**, 80 (1977).
19. R. L. Varner, W. J. Thompson, T. L. McAbee, E. J. Ludwing and T. B. Clegg, Phys. Rep. **201**, 57 (1991).
20. J. H. Dave and C. R. Gould, Phys. Rev. C **28**, 2212 (1983).
21. B. A. Watson, P. P. Singh and R. E. Segel, Phys. Rev. **182**, 977 (1969).
22. C. Mahaux, H. Ngô and G. R. Satchler, Nucl. Phys. **A449**, 354 (1986).
23. R. W. Finlay, W. P. Abfalterer, G. Fink, E. Montei, T. Adami, P. W. Losowski, G. L.Morgan and R. C. Haight, Phys. Rev. C **47**, 237 (1993).
24. P. E. Hodgson, Phys. Lett. **65B**, 331 (1976).
25. G. R. Satchler and W. G. Love, Phys. Rep. **55**, 183, (1979).
26. C. E. Aguiar, F. Zardi and A. Vitturi, Phys. Rev. C **56**, 1151 (1997).
27. F. Carstoiu, private communication.
28. R. C. Johnson, J. S. Al-Khalili and J. A. Tostevin, Phys. Rev. Lett. **79**, 2771 (1997).
29. A. Bonaccorso, I. Lhenry and T. Sïomijarvi, Phys. Rev. C **49**, 329 (1994).
30. A. Bonaccorso , Phys. Rev. C **53**, 849 (1996).
31. H. Laurent et al. , Phys. Rev. C **52**, 3066 (1995).  
Elke Plankl, These, Universite Paris VII, June 1999, unpublished, report IPNO-T-99-03.

**Table I.** Energy dependent optical model parameters.  $a_R=0.387\text{fm}$ ,  $r_I=1.368\text{fm}$ ,  $a_I=0.3\text{fm}$  at all energies.

| $\varepsilon_f$<br>(MeV) | $V_R$<br>(MeV)              | $r_R$<br>(fm)                       | $W_S$<br>(MeV)                      | $W_V$<br>(MeV)                   |
|--------------------------|-----------------------------|-------------------------------------|-------------------------------------|----------------------------------|
| 20-40                    | $38.5 - 0.145\varepsilon_f$ | $1.447 - 0.005(\varepsilon_f - 20)$ | $1.666 + 0.365\varepsilon_f$        | $0.375\varepsilon_f - 7.5$       |
| 40-120                   |                             |                                     | $16.226 - 0.1(\varepsilon_f - 40)$  | $7.5 - 0.02(\varepsilon_f - 40)$ |
| 120-180                  |                             |                                     | $8.226 - 0.07(\varepsilon_f - 120)$ | 5.9                              |

**Table II.** Initial state parameters in  $^{12}\text{Be}$ . Binding energies in MeV, asymptotic normalization constants  $C_i$  in  $\text{fm}^{-\frac{1}{2}}$ .

| $J, \pi$ | $l$ | $j$ | $ \varepsilon_i $ | $C_i$ |
|----------|-----|-----|-------------------|-------|
| $1/2^+$  | 0   | 0.5 | 3.32              | 2.45  |
| $1/2^-$  | 1   | 0.5 | 3.52              | 1.29  |

**Table III.** Breakup cross sections in mb from the initial states  $1/2^+$  and  $1/2^-$  in  $^{12}\text{Be}$  on  $^9\text{Be}$ , at several incident energies. Incident energies in A MeV,  $R_s$  in fm. Experimental data and shell model spectroscopic factors from [17].

| $J, \pi$ | $E_{inc}$ | $R_s$ | $\sigma_{str}$<br>TC | $\sigma_{str}$<br>eik | $\sigma_{diff}$<br>TC | $\sigma_{diff}$<br>eik | $\sigma_{-n}$<br>TC | $\sigma_{-n}$<br>eik | $\sigma_{exp}$ | $S_{SM}$ | $S_{TC}$ | $S_{eik}$ |
|----------|-----------|-------|----------------------|-----------------------|-----------------------|------------------------|---------------------|----------------------|----------------|----------|----------|-----------|
| $1/2^+$  | 20        | 6.5   | 35                   | 31                    | 45                    | 46                     | 80                  | 77                   |                |          |          |           |
|          | 40        | 6.1   | 41                   | 51.6                  | 31                    | 35                     | 72                  | 86.6                 |                |          |          |           |
|          | 60        | 5.8   | 43.5                 | 54.6                  | 24                    | 31                     | 67.5                | 85.6                 |                |          |          |           |
|          | 78        | 5.6   | 43                   | 54.8                  | 19                    | 24.7                   | 62                  | 79.5                 | 32(5)          | 0.69     | 0.65     | 0.51      |
|          | 100       | 5.4   | 42                   | 53                    | 13                    | 17.6                   | 55                  | 70.6                 |                |          |          |           |
| $1/2^-$  | 20        | 6.5   | 19                   | 16.5                  | 21                    | 22.7                   | 40                  | 39.2                 |                |          |          |           |
|          | 40        | 6.1   | 23.4                 | 29.6                  | 16.3                  | 18                     | 39.7                | 47.6                 |                |          |          |           |
|          | 60        | 5.8   | 27.2                 | 32.7                  | 13                    | 15.9                   | 40.2                | 48.6                 |                |          |          |           |
|          | 78        | 5.6   | 28                   | 34                    | 11                    | 13                     | 39                  | 47                   | 18(3)          | 0.58     | 0.54     | 0.45      |
|          | 100       | 5.4   | 28.4                 | 33.7                  | 8.4                   | 9.7                    | 36.8                | 43.4                 |                |          |          |           |

### Figure Captions.

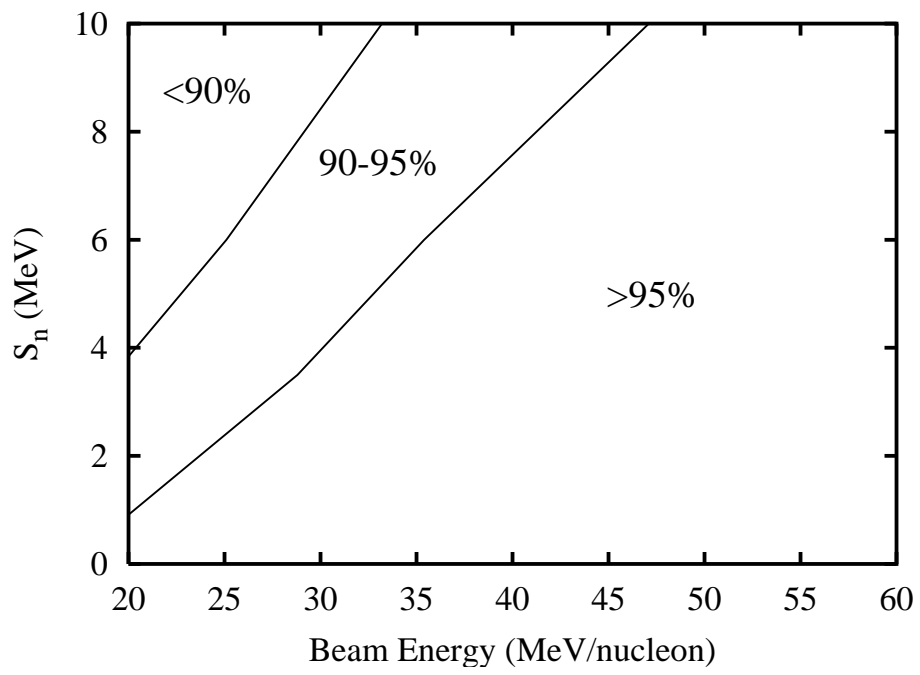
**Fig.1** Ratio of phase space integrals with and without momentum cutoff, for a  $d$ -wave neutron wave function. The effect of the cutoff is to include less than 90%, between 90% and 95% and more than 95% of the initial momentum distribution as marked on the figure.

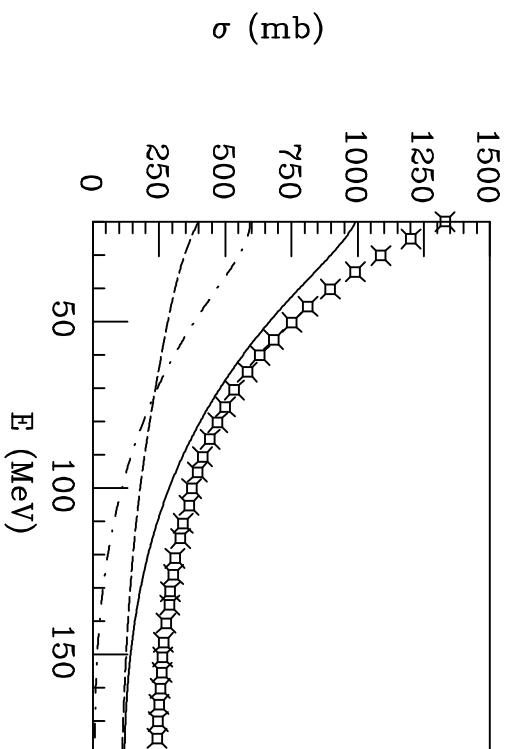
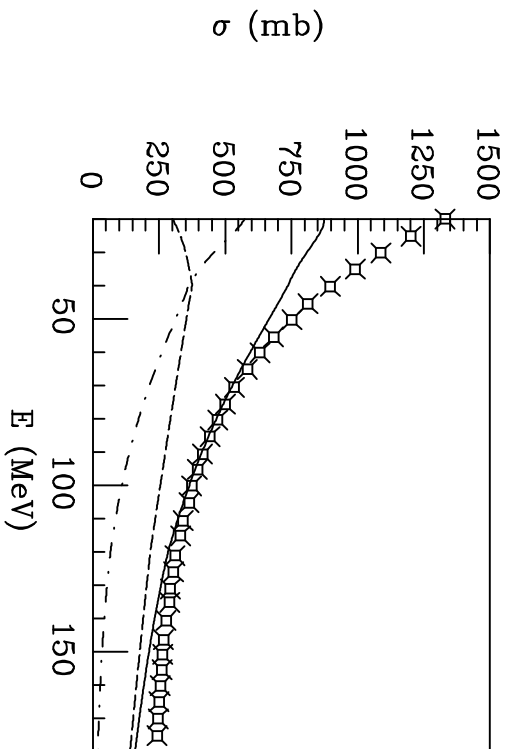
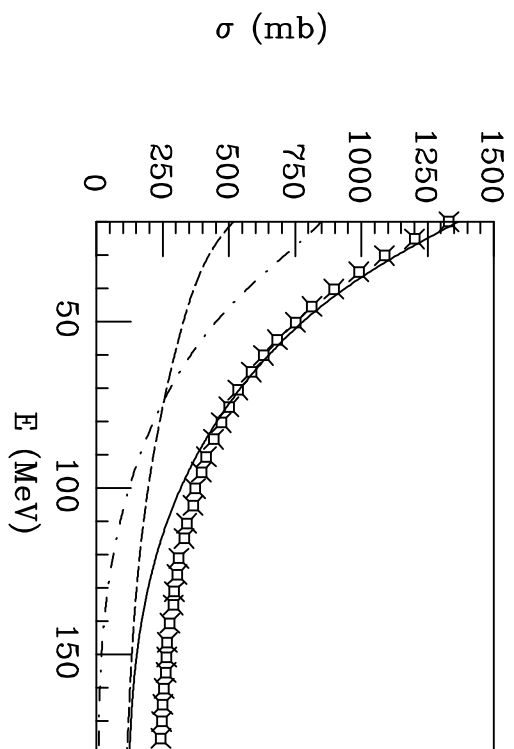
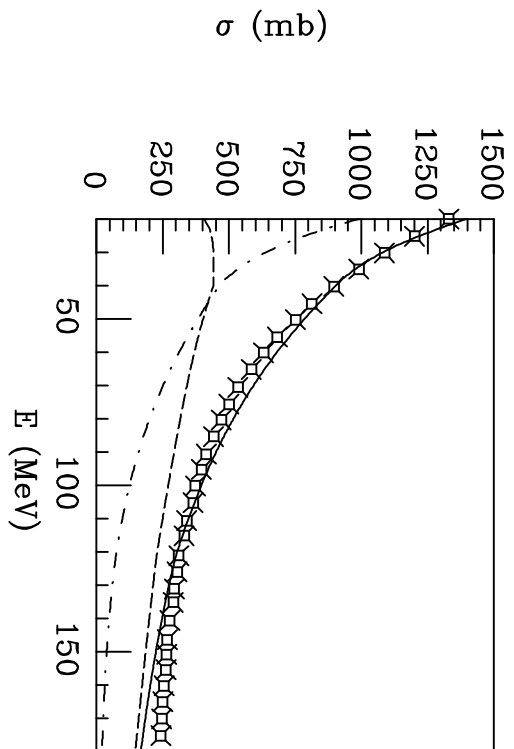
**Fig.2** Top left: Experimental cross sections for neutron scattering on  ${}^9\text{Be}$  together with the optical model cross sections using the potential of Table I. The full curve is the total cross section, the dotdashed curve is the elastic cross section while the dashed curve is the reaction cross section. Bottom left: same quantities calculated in the eikonal approximation. Top and bottom right: the same quantities calculated with the Varner potential.

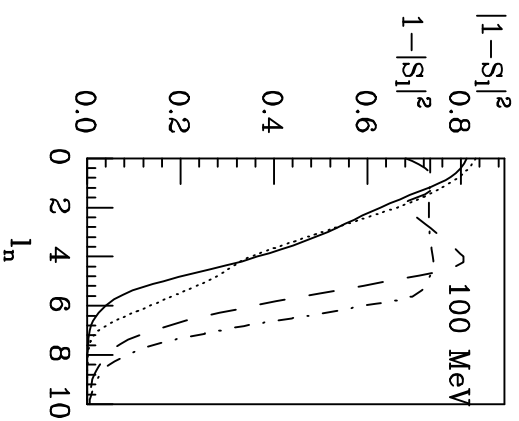
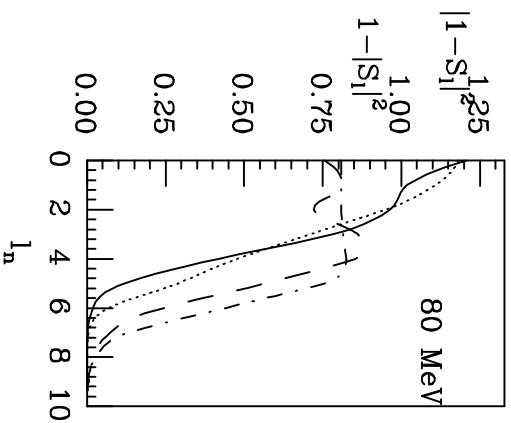
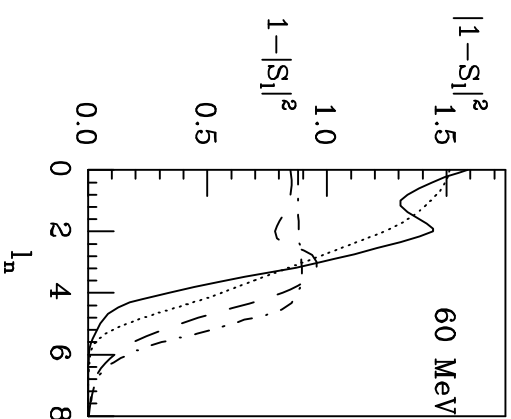
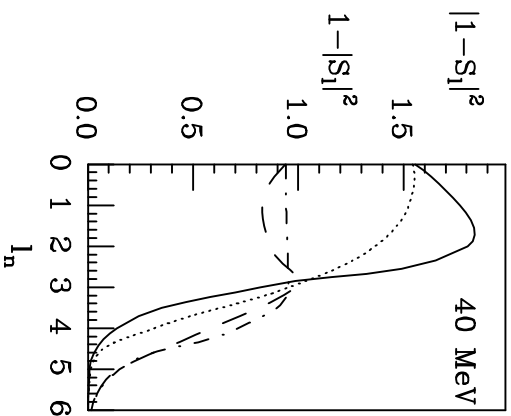
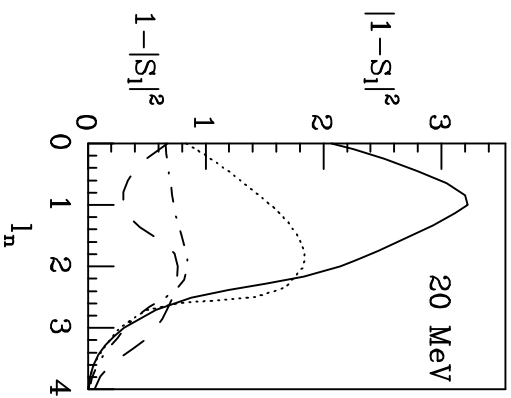
**Fig.3** The behavior of the term  $|1 - S|^2$  and of the transmission coefficient  $1 - |S|^2$  calculated by the optical model (solid and dashed line respectively) and by the eikonal approximation (dotted and dotdashed line). Results are shown as a function of the angular momentum  $l_n$ . In the case of the eikonal calculations the semiclassical relation  $l_n + 1/2 = kb_n$  was used to make the connection with the neutron impact parameter. Results are given at incident energies ranging from 20 to 100 MeV.

**Fig.4** Total breakup probabilities from the  $1/2^-$  state in  ${}^{12}\text{Be}$ , as a function of the ion-ion impact parameter for diffraction obtained in the TC calculation by the solid line. The dashed line is for the stripping. Energies are as in Fig. 3. Dotted and dotdashed lines are diffraction and stripping probabilities from the eikonal calculation.

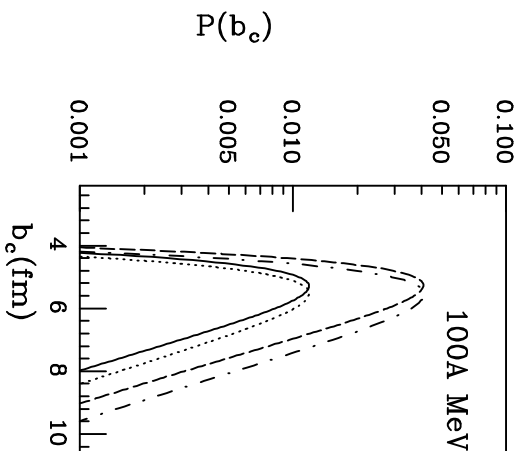
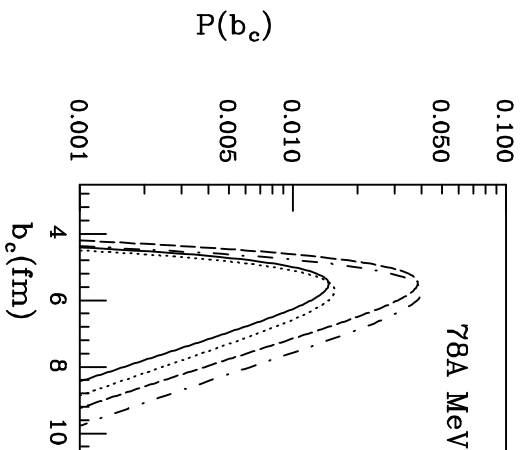
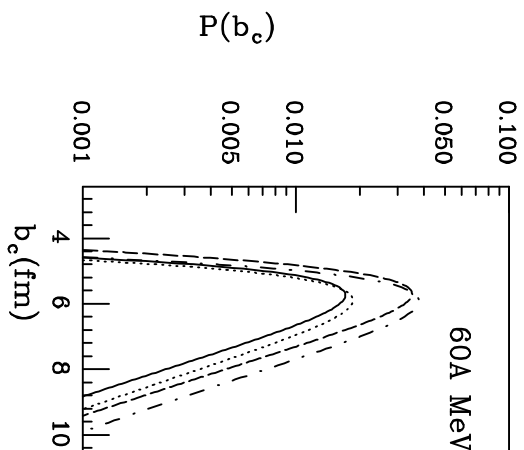
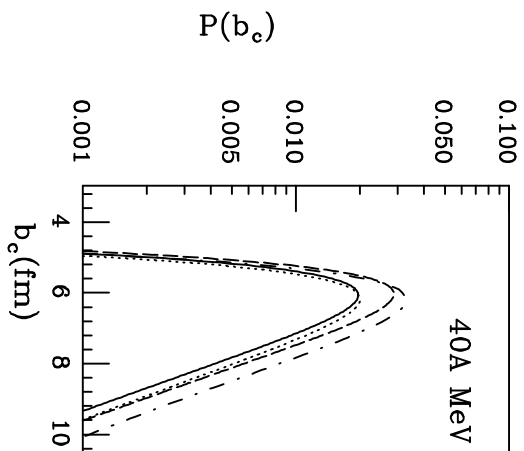
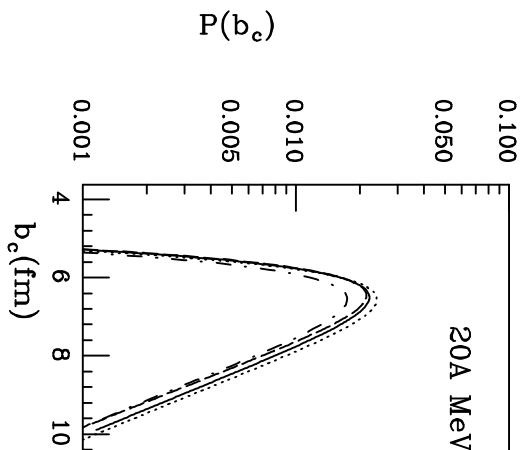
**Fig.5** The integrand function of the diffraction (a), and stripping (b) term of Eq.(11) after  $k_z$  integration, full curve, obtained from the realistic bound state wave function and the corresponding terms, diamonds, in the sum over partial waves of Eqs.(5,6) in the case of the incident energy of 78A MeV. Crosses are the results of a calculation of Eq. (11) in which the eikonal phase shifts have been substituted by the optical model phase shifts according to Eq.(27). All calculations done at fixed impact parameter  $b_c = 5.6\text{fm}$  between the projectile and target.







-----  $|1-S_l|^2$  opt. mod  
 .....  $|1-S_l|^2$  eikonal  
 - - - - -  $1-|S_l|^2$  opt. mo  
 - . - . - .  $1-|S_l|^2$  eikonal



- - - - - diffraction TC.  
 ..... diffraction eikon  
 - - - - - stripping TC  
 - . - . - . stripping eikon

